Arbitrary-Waveform Electro-Optical Intracranial Neurostimulator with Load-Adaptive High-Voltage Compliance

Hossein Kassiri, Fu Der Chen, M. Tariqus Salam, Michael Chang, Behraz Vatankhahghadim,
Peter Carlen, Taufik A. Valiante, Roman Genov

Abstract—A hybrid 16-channel current-mode and 8-channel optical implantable neurostimulating system is presented. The system generates arbitrary-waveform charge-balanced current-mode electrical pulses with amplitude ranging from 50 μA to 10 mA. An impedance monitoring feedback loop is employed to automatically adjust the supply voltage, yielding a load-optimized power dissipation. The 8-channel optical stimulator drives an array of LEDs, each with a maximum of 25 mA current amplitude, and reuses the arbitrary-waveform generation function of the electrical stimulator. The LEDs are assembled within a custom-made 4×4 ECoG grid electrode array, enabling precise optical stimulation of neurons with a 300 μm pitch between the LEDS and simultaneous monitoring of the neural response by the ECoG electrode, at different distances of the stimulation site. The hybrid stimulation system is implemented on a mini-PCB, and receives power and stimulation commands inductively through a second board and a coil stacked on top of it. The entire system is sized at 3×2.5×1 cm^3 and weighs 7 grams. The system efficacy for electrical and optical stimulation is validated in-vivo using separate chronic and acute experiments.

I. INTRODUCTION

Epilepsy is a chronic neurological disorder characterized by recurrent seizures. There is a profound need to better understand epileptogenesis and seizure onset since nearly one-third of all epilepsy patients remain refractory to conventional therapeutic interventions [1]. Electrical neuro-stimulation is an established effective drugs-alternative treatment option for a variety of neurological disorders. High-frequency ($\geq$ 130 Hz) and low-frequency (0.5-5 Hz) deep-brain and cortical stimulation have been shown to be effective in epilepsy, depression, neurodegenerative diseases, and movement disorders [2]–[10]. For epilepsy, while both have resulted in suppressing the seizure duration and propagation [4]–[6], the low-frequency stimulation is often preferred due to the lower power requirement and subsequently lower risk of tissue damage.

In [5] the authors have shown the effectiveness of the low frequency stimulation in a closed-loop configuration. It is also shown that low-frequency neurostimulation causes a short-term synaptic depression of excitatory neurotransmission
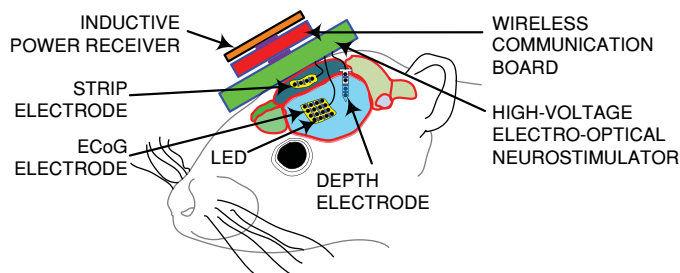
Fig. 1: Envisioned implantation configuration of a wireless electro-optical neurostimulator and mounting configuration of its three main components.

[11], and recently we have reported its effect in reduction of overall neural excitation at seizure onset [12]. Our group has also demonstrated that the seizure can be interrupted at an earlier stage before its full progress and propagation contralaterally, both in short-term [23] and long-term [13] animal experiments. Despite all the progress in the recent years, the exact mechanism behind neuromodulation using electrical stimulation in many cases remains unknown, in part due to the lack of a proper tool enabling cell-type-selective neural excitation or inhibition in addition to simultaneous high-resolution spatiotemporal neural recording.

Electrograph seizure onset has been correlated with augmented GABAergic neurotransmission in in-vivo [25], in-vitro [26]–[29], and clinical [30], [31] investigations. Convergence from both rodent and human studies indicate GABAergic circuitry is responsible for transition into electrographic seizures with a low voltage, fast activity (LVF) onset pattern [32]–[35]. It has been shown in both acute and chronic epilepsy models that prior or during an epileptic seizure, GABAergic activity is either preserved [36] or increased [37]–[40]. Also in [34], [41], the authors have demonstrated that a 300–1000 ms optogenetic stimulation in in-vitro 4-aminopyrmidine (4-AP) seizure model, which results in sustained activation of GABAergic interneurons can initiate epileptic ictal events. Our group have recently shown in an in-vivo 4-AP seizure model that optogenetic activation of GABAergic interneurons in layer 2/3 of the neocortex is sufficient to trigger LVF ictal events [42].

This is only one of the several examples of the relatively-new optogenetic neurostimulation technique that has opened an avenue for better understanding of mechanisms of neural function. Optogenetic cell-type-specific modulation of neuronal activity opens up the prospect of initiating or preventing abnormal brain states that result in certain neurological conditions [15]. Unlike electrical stimulation, optogenetic stimulation selectively modulates neuronal activity in a local neural network and this modulation does not generate artifacts in the

TABLE I: State-of-the-art implantable/wearable systems for optical/electrical stimulation of the brain.

	JSSC'18 [16]	TBCAS'18 [17]	ISSCC'18 [18]	JSSC'12 [19]	ESSCIRC'16 [20]	JSSC'15 [21]	THIS WORK
Stim. Waveform.	Optical Biphasic	Optical Biphasic	Optical Biphasic	Electrical Arbitrary	Electrical Arbitrary	Opt./Elec. Arbitrary	Opt.+Elec. Arbitrary
System Size	N/R	$4.23 \times 2.3 \ mm^2$	$8 \times 14 \ mm^2$	N/A	$2 \times 2 \times 0.7 \ cm^3$	N/R	$3 \times 2.5 \times 1 \ cm^3$
Wireless Data	Yes	No	Yes	No	Yes	Yes	Yes
Wireless Power	No	No	Yes	Yes	Yes	Yes	Yes
Max VDD (V)	1.2	5	5	20	20	± 2.1	24
Current Range (mA)	<35	<1.1	<10	0.003-1	0.023-95	0.012-1.5	0.05-10
Opt. Ch. Count	4	6	16	0	0	4	8
LED Separation(μm)	250	250	250	N/A	N/A	540	300
In-vivo Validation	Yes	Yes	Yes	No	No	Yes	Yes
Elec. Ch. Count	0	0	0	2	4	4	16
Adaptive Power Efficiency	No	No	No	Yes	Yes	Yes	Yes
Max Power Saving (%)	N/A	N/A	N/A	64.7	68.5	N/R	70

recording.

Based on our success in using optogenetic and electrical stimulation for initiating and aborting epileptic seizures, respectively, it seems that a combination of electrical and optical stimulation such as the system presented in Fig.1, is a potent novel technique for better understanding of the brain function and dysfunction, and for generating optimal brain modulation for treating neurological disorders.

In this paper we present a combined 16-channel current-mode and an 8-channel optical-mode neural stimulating system. Both stimulators can generate arbitrary waveforms with up to 10 bits of resolution. To ensure optimum power consumption, a digital low-power load-adaptive supply controller is embedded in the system. Additional circuits are added to the system to ensure safe and charge-balanced stimulation pulses are delivered to the brain. This paper extends on an earlier report of the principle and demonstration in [24], and offers a more detailed analysis of the design and additional experimental results characterizing the circuit implementation and in-vivo validation.

The presented device can initiate and suppress electrographic seizures in the whole intact brain of transgenic mice expressing channelrhodopsin-2 (ChR2) in all sub-types of GABAergic interneurons. The device exploits the spatial and temporal control of GABAergic interneuronal activation with optogenetics in a focal seizure model to successfully initiate electrographic seizures on-demand with a single photostimulus (473 nm; <1 s). The transition into seizure using the light pulse as the temporal reference point for seizure onset was then recorded. Intriguingly, the electrographic seizures in the in vivo 4-AP model was reminiscent of the commonly observed electrographic seizures with LVF onset patterns from patients with medically refractory temporal lobe epilepsy (TLE) [35]. The device can be simply adapted to employ other transgenic strains of mice to target different neuronal populations in a variety of other in vivo seizure models. In terms of hardware, the adaptation only requires simple re-soldering of the LEDs with a different color (wavelength). In terms of software/firmware changes, the programmable design allows for any change in stimulation pulse parameters (e.g., delay, amplitude, duty cycle, width, etc.) by simply reprogramming the controlling

FPGA. The ability to study clinically-relevant electrographic seizures in the completely intact neuronal network of adult mice allows us to avoid issues related to the young age of animals [43] or slicing procedure [44] associated with brain slice experiments.

The rest of the paper is organized as follows. Section II discusses the top level system architecture of the wireless dual-mode neurostimulator. Section III presents the design implementation of the key functional blocks in the system. Section IV describes the architecture of the digital controller used to control the system mode of operation and to ensure optimal power consumption. Section V presents the design and fabrication details of the electrode used for multi-channel dual-mode stimulation and electrical recording. Section VI presents electrical experimental results of the individual blocks as well as the full system. Section VII presents in-vivo online animal results for both optical and electrical stimulations.

II. SYSTEM ARCHITECTURE

Due to the above-mentioned benefits of optical stimulation of neuronal circuits in studying neurological disorders, it has rapidly gained popularity in recent years. Over the past few years, there have been several implantable and miniaturized-wearable devices reported in the literature capable of multi-channel optical stimulation. Depending on the targeted application, these systems are implemented with different channel count, physical size/shape, and a wide range of power consumption. Table I presents some of the most recent reported works in the literature with their system-level parameters compared to the presented design in this paper. Additionally, given the importance of electrical stimulation in control of neurological events, as described in the previous section, the table also includes designs that feature multi-channel electrical stimulation that particularly feature a power efficiency boosting scheme. The importance of such feature, especially for systems with a high supply voltage is described in the rest of this section.

Various circuit configurations have been reported in the literature for electrical stimulation. Voltage-controlled stimulation (VCS) [45], current-controlled stimulation (CCS) [22], [23] and switched-capacitor charge-base stimulation (SCS) [21] are
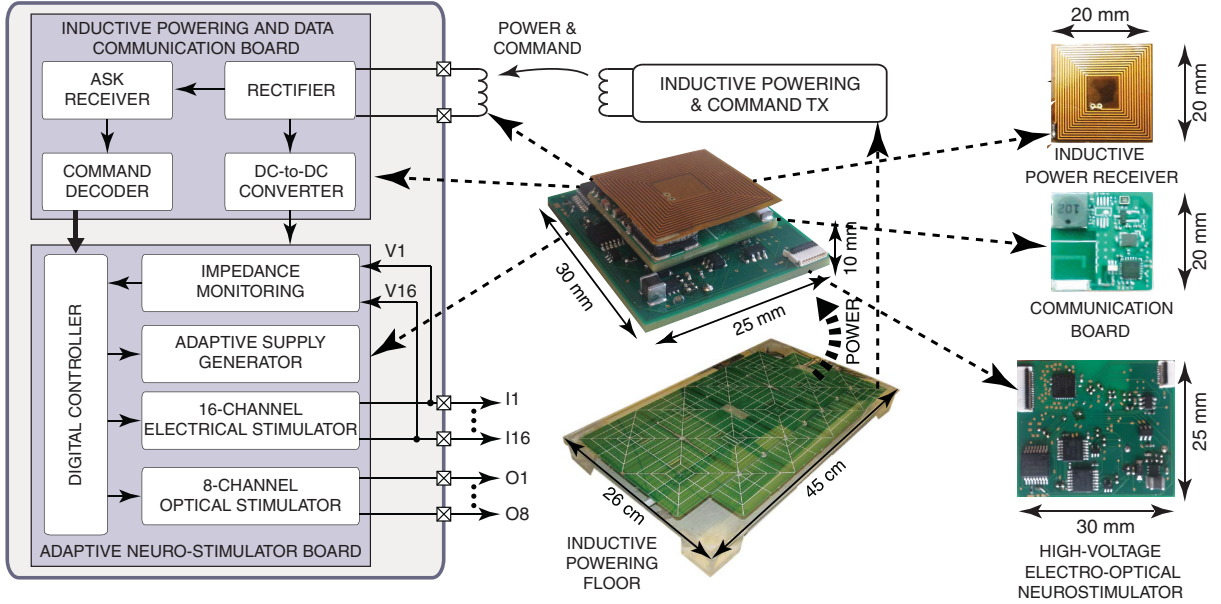
Fig. 2: Simplified block diagram and physical view of the inductively-powered electro-optical stimulating system.

the three existing methods to provide electrical stimulation to the body. VCS can not control the amount of the injected charge during the stimulation which could lead to sub-optimal results and tissue damage. SCS provides a precise control on the delivered charge to the tissue, but has the disadvantage of limited control over the stimulation pulse shape. Current-based stimulators, on the other hand, have excellent control of charge injected into the tissue and can deliver a precisely-programmed current pulse shape.

Despite the advantages, current-controlled stimulators typically suffer from poor power efficiency compared to both VCS and SCS. This is because the supply voltage of these stimulators is set to accommodate sufficient headroom voltage for the worst-case scenario, which is stimulating with the highest-amplitude current into the largest possible tissue impedance. For a rectangular current-mode stimulation pulse with an amplitude of I_{stim}, the minimum required supply voltage is [19]:

$$VDD_{min} = I_{stim} \cdot R_{elec} + \frac{I_{stim}T_{stim}}{C_{elec}} + V_{headroom} \quad (1)$$

where R_{elec} and C_{elec} are resistive and capacitive components, respectively, T_{stim} is the maximum stimulation period, and $V_{headroom}$ is the minimum required headroom voltage. This equation shows that the required voltage compliance for a neurostimulator is set by stimulation current amplitude and the electrode impedance. Operating with maximum supply voltage when stimulating with lower-than-maximum current amplitudes or into smaller-than-maximum tissue impedances, results in a significant portion of the consumed power being wasted. The power loss becomes even more significant when high voltage compliance (i.e. >10V) is needed to provide sufficient headroom for stimulation.

To address the power loss issue, some power adaptive neuro-stimulators are reported [46]–[48]. The common goal of all these designs is to set the supply voltage at the minimum

required compliance. This demands for the supply voltage to be adaptive to not only the stimulation current amplitude that is set by the user, but also to the electrode impedance variations that happen during the experiment.

In [46], the authors have reported an energy efficient charge-balanced voltage-mode neurostimulator. To guarantee a charge-balanced operation, the stimulation current is sensed and compared with a reference value, and if needed, the electrode voltage is changed to adjust the current to the desired value. Using this method, the electrode voltage is always set at the exact required value that is demanded by the stimulation current and electrode impedance. However, in addition to problems associated with voltage-mode stimulators, this method require a DC-DC converter with bulky external components in each channel, which prevents it from being scaled to multiple channels.

In [47] a fully integrated DC-DC converter is designed to set the supply voltage slightly higher than the minimum required electrode voltage for a particular stimulation current. Despite being fully integrated and scalability, the supply is only adaptive to current variations and does not operate as expected if electrode impedance varies. Also unlike [46], the supply voltage has only 4 different levels (3V, 6V, 9V, 12V) which result in a maximum of 50% power saving.

In [48], the authors have reported an energy efficient stimulator with adaptive supply voltage. The stimulator essentially mimics the electrode voltage that is expected for a particular current. The supply voltage variation is done by tapping into different terminals of a secondary power telemetry coil which has the advantage of not needing a DC-DC converter. However, there are only a few possible voltage levels. This means that the stimulation current is not controlled precisely. Also the reported design does not take electrode impedance variations into account.

Fig. 2 shows a simplified block diagram and system break-

TABLE II:
Power breakdown of the off-the-shelf components used

Components	Company	Model	Quiescent Power(mW)
Boost Converter	TI	TPS61040	3.4
DAC	Maxim	MAX5363	0.14
ADC	TI	ADC081C021	1.2
Current Source	NXP	PSSI2021SAY	-
Digital Pot.	Microchip	MCP41HV51	0.24
HV SPST	Maxim	MAX4662	0.01
HV MUX	ADI	ADG5206	0.01
LED Driver	Semtech	SC620	4.5
Regulator	TI	TPS73701	2.1
Regulator	TI	TLV711	3
FPGA	Actel	AGL060V5-cs121	0.35
Crystal	Epson	SG-210	2.2

down of the adaptive-supply electro-optical neurostimulator. The system is comprised of two board and an inductive coil stacked on top of each other. Dual-mode neurostimulation is performed by the first board, on the bottom, and the second board, in the middle, and the coil are used to provide energy and commands to this board.

The system has 16 electrical and 8 optical stimulation channels. All channels generate independently-programmed arbitrary waveforms for hybrid neurostimulation. The system connects with both ECoG electrodes and LED-arrays that are implanted over the brain cortex surface. To minimize the power consumption, tissue impedance variations seen at each electrode are continuously monitored and fed to a digital controller that adjusts the supply voltage as well as the DC level of the reference electrode to keep the voltage compliance at the minimum required.

Fig. 2 also depicts how the stimulator board is connected to the wireless power and command receiver board through a vertical connector. The wireless board rectifies and regulates inductively-transmitted power that is sent by a cellular inductive powering rodent cage floor [53], and received by the receiver coil mounted on an animal. The inductive link provides power at the maximum distance of 15 cm. The system utilizes the same inductive link to receive configuration commands.

III. DESIGN IMPLEMENTATION

Fig. 3 shows a simplified block diagram of the neurostimulator board. The figure also shows the top and bottom views of the board with all the major components labeled. The system is entirely built using commercial off-the-shelf components, including a low power FPGA, digitally controlled current drivers, a programmable boost converter, an 8-channel digitally-controlled LED driver, a crystal oscillator, and a number of flexible flat cable (FFC) and vertical connectors for connection to the stimulation electrode arrays and wireless power/data communication board, respectively. The digital controller implemented in the low-power FPGA is used to control the system mode of operation, channel selection, stimulation parameters for each channel (e.g. waveform shape, amplitude, frequency, etc.), and optimal supply voltage. Table II summarizes the off-the-shelf components used in this

board and their corresponding power consumption in normal operation mode.

A. Power adaptive feedback

As mentioned, to avoid the poor power efficiency of the current-controlled stimulation method, the system is designed to have an adaptable supply voltage to the stimulation condition. For optimal operation, the supply voltage should always be set to the minimum required voltage compliance, which is calculated based on the stimulation current amplitude and instantaneous electrode impedance. Unlike the stimulation current amplitude that is known (e.g., set by a clinician), the tissue impedance could change significantly during the experiment and must be continuously monitored.

In this design, an 8-bit low-power ADC is used to sample the voltage difference between the stimulating and reference electrodes, quantize it, and send it to the digital controller implemented on the FPGA to determine the minimum supply voltage required. While the circuit works with a practical maximum sampling rate of 180ksps, we validated the performance of the impedance monitoring module in the lab at lower rates of 50ksps, 10ksps, and 1ksps. Due to the expected very slow variations of interface impedance, for the clinical experiments, we observed that the device works properly with a significantly lower sampling rates (e.g., <100 sps), yielding a significantly lower dynamic power consumption for the module.

Initially, the supply voltage is set to the maximum since the electrode-tissue impedance is unknown. After startup, the system operates as a normal stimulator unless the digital controller detects a non-optimal (shortage or excess of VDD) supply voltage. To avoid unnecessary changes of the supply voltage due to high-frequency noise or interference, a tolerance window is defined below the current VDD value with upper and lower thresholds. The controller decides to change the supply voltage only if the sampled voltage passes either threshold for a certain period of time.

Once a decision is made, proper commands are sent to a boost converter (through a low-power digital-to-analog converter (DAC)) responsible for altering the supply voltage. The adjustable boost converter receives a 3.3V DC from the wireless board as an input and can generate up to 24V depending on the command it receives from the FPGA. Such high supply voltage provides a large voltage headroom for current drivers and consequently enables higher stimulation currents. Considering 1.5-2V drop on current sources (I_{source} and I_{sink}), for a typical 1 kΩ tissue resistance, the system can provide up to 10 mA current. The updated supply voltage will be positioned at 1.5V higher than the sampled voltage in order to accommodate the required headroom voltage for the current source. Also, if the new voltage is higher than what the boost converter can supply, the FPGA generates an overflow signal to notify the user. Once the stimulation for the channel is completed, FPGA saves the last voltage level into the channel profile so that the next iteration starts with the proper supply voltage.
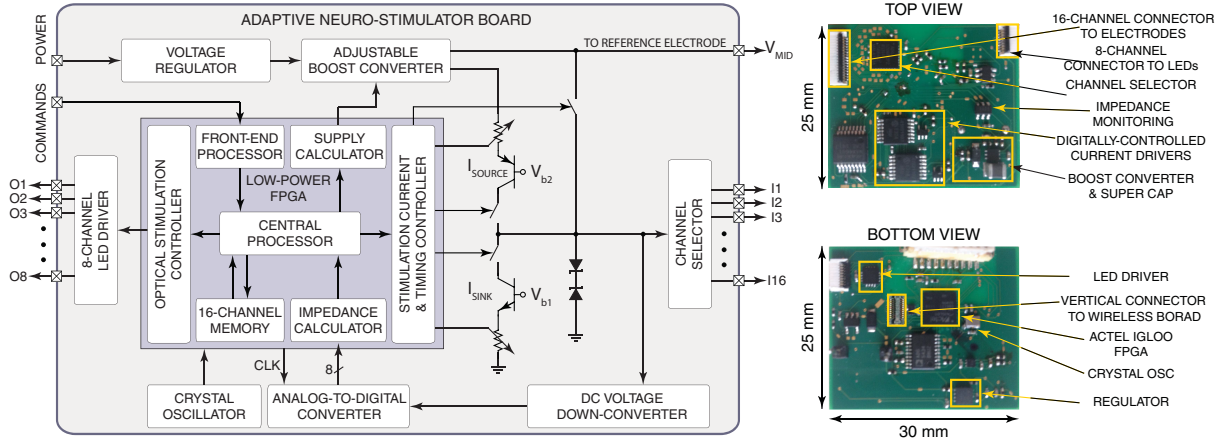
Fig. 3: Simplified block diagram of the power-adaptive high-voltage electro-optical stimulator board.

B. Programmable Pulse Shape

The results in [51], [52] show that the pulse shape significantly affect the delivered charge to the tissue as well as stimulation-induced tissue damage. It is also shown that with the optimal waveform, the required current amplitude can be reduced which leads to lower power consumption [21]. For the current-mode stimulation, common-base BJT current drivers are controlled using digitally-adjustable potentiometers connected in series with the emitter. The $50\mu A$ minimum current amplitude and the amplitude adjustment resolution are set by the maximum resistance of the potentiometer as well as the number of digital bits controlling it. To show-case the maximum possible stimulation current that can be delivered with this system, we chose a 10-bit digital potentiometer with a maximum of $50k\Omega$ resistance. This yields a current range of 50 μA to 10 mA. However, for applications that require smaller maximum current amplitudes in the order of hundreds of micro-Amperes, the discrete design of the presented system allows for simple replacement (i.e., re-soldering) of the digital potentiometer IC with a model that has a higher maximum impedance. For example, the Analog Devices' AD5241 digital potentiometer chip provides a maximum of $1M\Omega$ resistance with similar resolution, which translates to $20\times$ down-scaling of the current range to approximately 2.5-500μA. The digital potentiometer itself is controlled digitally by the FPGA and has 1024 positions. To control duty-cycle of the stimulation waveform, a timer is implemented on the FPGA to keep track of the stimulation duration.

C. Safety Features

To avoid charge accumulation, the current-mode stimulator is always programmed for equal overall charges flowing in and out of the tissue. However, the mismatch between the anodic and cathodic currents could result in a residual charge that must be removed. As shown in Fig. 3, a discharging path to the reference electrode V_{MID} is utilized to compensate for the charge mismatch following an stimulation episode. The same switch is used to discharge accumulated charge on the ac-coupling capacitor due to switches leakage current.

A sudden high current could inrush into the tissue when switching the stimulation path on, which could alter the stimulation effect or damage the tissue. A voltage limiter built using Zener diodes is employed in the system to prevent a high current flowing into the tissue. When high current is flowing into the electrode, it will induce a high voltage. Once the voltage across electrode reaches a certain voltage, the Zener diode will fall into the breakdown region, diverting the high current into the ground.

D. Optical Stimulation

For the optical stimulation, an LED light source is driven by a current as governed by its exponential I-V relationship. Increasing stimulation current does not change the LED junction voltage, and consequently does not demand for higher supply voltage. In this design, a 3.3V supply voltage is sufficient to drive the LEDs with the targeted maximum light intensity. As a result, independent electrical and optical stimulation not only enables simultaneous modes of operation, but also saves a significant amount of energy that would be wasted in LEDs otherwise. An 8-channel digitally-controllable LED driver is utilized to provide up to 25 mA current to the LED array and is supplied with a fixed 3.3V voltage.

E. Wireless Powering and Communication

For an implantable/wearable system designed for rodent studies, power and configuration commands should ideally be provided wirelessly to avoid bulky and heavy batteries and wires [50]. The inductive link provides the operating power continuously with the maximum distance of 15 cm away from the transmitter. The power carrier is amplitude shift-keyed to communicate the configuration commands from a computer to the implantable system using the same wireless link. A 470 mF super capacitor is utilized that gets charged during the idle phase and provides stable supply voltage during stimulation phase for a maximum of 2 minutes continuous pulse-train with the maximum signal amplitude. A comparator is utilized to monitor the power usage of the system. If the voltage of the super capacitor falls below 3.6 v, the FPGA will stop the stimulation to avoid abnormal behavior under low power conditions. The inductive powering system operates at 1.5MHz.

The receiver coil is designed to provide sufficient energy to the implant that is mounted on animal's back or head (<15cm) during its normal operation. Considering the above requirements, the physical size of the receiver coil is then
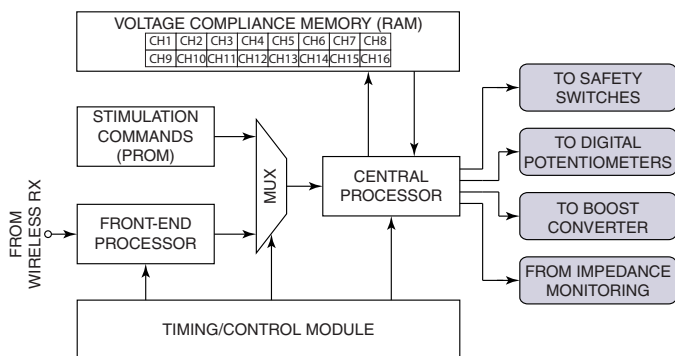
Fig. 4: System architecture of the digital controller implemented on the FPGA.

TABLE III:
FPGA resource utilization

Parameter	Value
Core Logic Elements	486
Sequential Logic Elements	339
Combinational Logic Elements	147
Number of Inputs/Outputs	22
Flash ROM	1
RAM Blocks	4
Logic Level	3.3V
Max Clock Frequency	32 MHz

(a)

(b)   (c)

Fig. 5: Flexible ECoG grid: (a) Layers of ECoG (not to scale), (b) fabricated flexible ECoG electrode array (top view), and (c) LEDs assembled within the dual-layer flexible ECoG electrode array (opcog) and blue light passing through the opcog from LED 1 (bottom view).

minimized to yield smallest possible form factor. The power transmitter floor that is comprised of two overlapped 2×4 arrays of coils sits under the animal cage. The maximum coil separation of 15 cm is chosen as it is the farthest possible that the implant gets when it is mounted on top of animals head, even when the mouse is standing in the cage.

IV. DIGITAL SYSTEM ARCHITECTURE

The system architecture of the digital system implemented on the FPGA is shown in Figure 4. The controller is comprised of a front-end processor, a central processor, two memory modules, and a timing/control module. The front-end processor can decode commands including start, pause, and stop stimulation, configuring the pulse shape, channel selection, and mode of operation. These commands activate the central processor to generate proper signals to different blocks on the board. Alternatively, these commands can be saved into the FPGA memory and played during stimulation. The pulse shape configuration commands include pulse shape information of each channel, channel location, stimulation period, number of repetition, start time, width of pulse-train and amplitude. The receiver stops accepting data once the end of command bit is detected. The protocol also contains reserved bits for checking data integrity. The benefit of collecting all the configuration parameters at the startup period is to reduce the use of communication system during stimulation.

When the stimulation is triggered, the central processor decodes the received data following a custom protocol. The first word informs the central processor the number of pulses used to define the desired pulse shape. It also tells the central processor which stimulation channel to turn on. After acquiring these information, the central processor decodes one pulse command at a time. The current level encoded in the pulse command will be sent to potentiometer controller. The
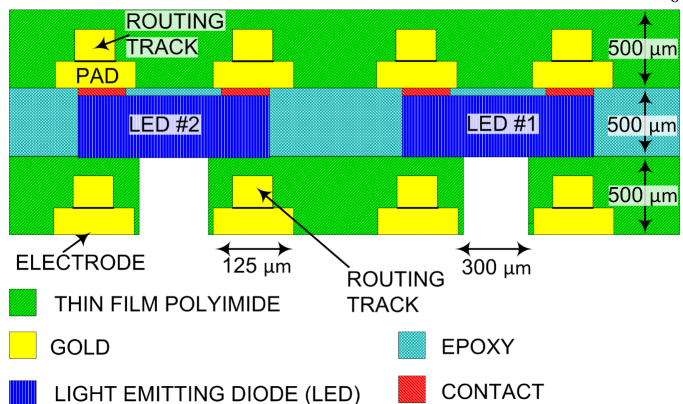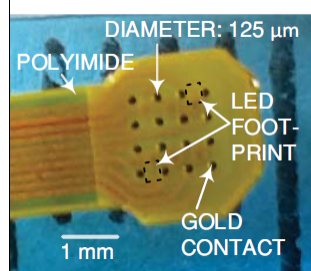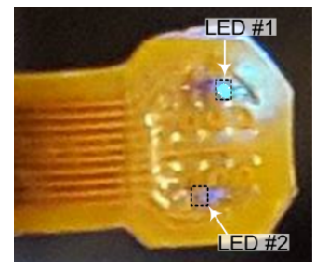
potentiometer controller converts the data to the specified SPI protocol and sends it to the IC component. The potentiometer IC requires 10 μs to receive the data and to stabilize the resistor. The minimum pulse width for each stimulation pulse is therefore 10 μs due to the set-up constraint. During stimulation, the time tracker, embedded in the timing module, turns on and continuously compares the internal timer with the specified pulse width. When the pulse width is reached, another line of pulse command will be decoded in the central processor. This process continues until the central processor decodes the same number of pulse commands specified in the first line of pulse shape command set, indicating the completion of the arbitrary-waveform pulse. The last command for the pulse shape defines the wait time between two consecutive pulses. During this time, the system is being set to idle to reduce the power consumption. Also in the idle state, the stimulation channel is grounded to reestablish charge balancing. At the end of every channel stimulation, the highest voltage recorded by the ADC is saved in the 16-channel voltage compliance memory so that the information can be utilized at the start of next repetition of stimulation to save power. Table III summarizes the FPGA resource utilization, logic level, and clock frequency.

V. ELECTRODE DESIGN

The ECoG electrode was fabricated on a Polyimide sheet of thickness 100 μm. Polyimide material was chosen for its flexibility, chemical stability, and biocompatibility properties. For
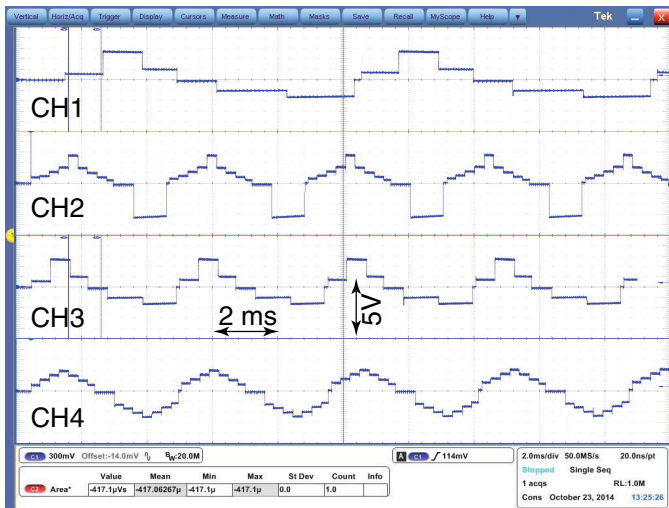
Fig. 6: Four experimentally-measured independent arbitrary waveforms generated simultaneously by the neurostimulator for an nominal 1kΩ load.

Fig. 8: System power consumption with adaptive (red) and fixed (black) power supply, for different load impedance values.
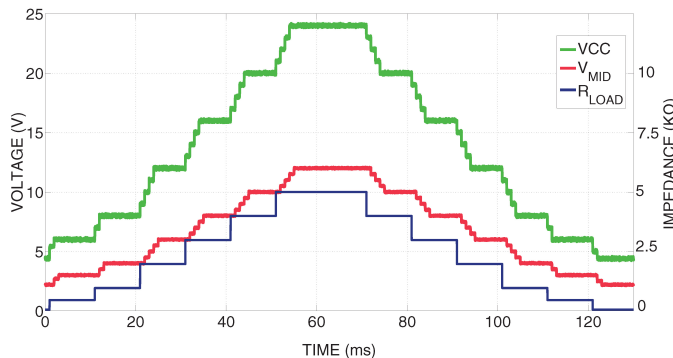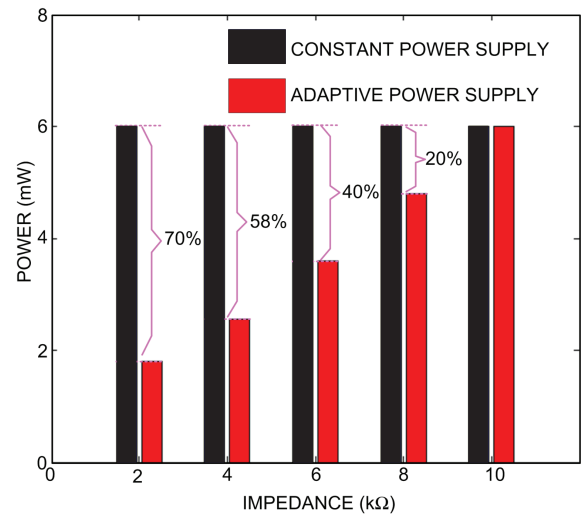

Fig. 7: Experimentally-measured voltage waveforms of the adaptive supply and reference voltage. The system keeps the supply voltage at the optimum value for a 2mA stimulation current while load impedance varies.

the electrode material, gold was chosen for its biocompatibility and compatibility with the micro-fabrication process. First metalization layer was formed (800 nm) using DC sputtering deposition and was patterned using photolithography and wet etching to create the routing tracks (Fig. 5(a)). The first metalization layer was used for the electrode connection routing. The second layer of Polyimide was spin coated and another metalization layer was deposited similarly for the electrode contact. Light emitting diodes (LED) were soldered to a pair of contacts of another ECoG electrode array and sandwiched in between the two ECoG electrodes using epoxy. The fabricated ECoG electrode and LEDs are shown in Figs. 5(b) and (c).

VI. ELECTRICAL MEASUREMENT RESULT

Fig. 6 shows an example of four experimentally-measured simultaneously-generated electrical stimulation waveforms. The waveforms are acquired from the stimulator channels output connected to 1kΩ loads in a bench-top test setup. The electrode-tissue interface impedance is a factor of the electrode physical size and the frequency of stimulation. For the stimulation electrodes that were used in our experiments and for the targeted stimulation frequency (5-30 Hz), 1kΩ is chosen as a typical value.
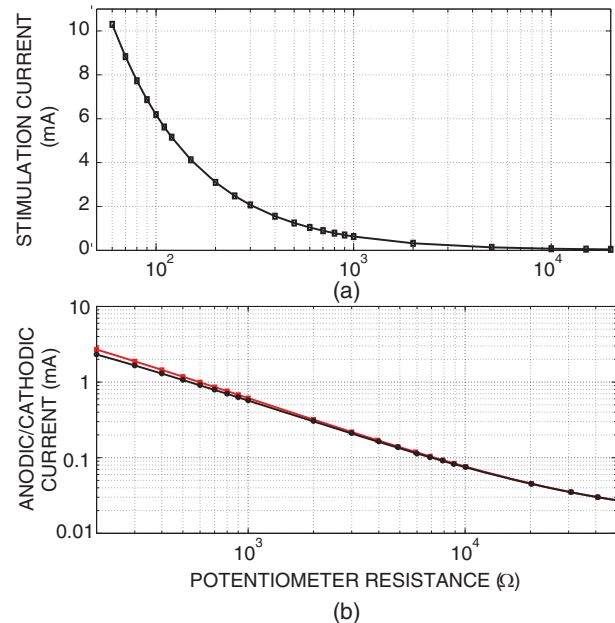

Fig. 9: Experimentally-measured (a) stimulation current, and (b) anodic and cathodic current amplitudes, for different values of the digitally-controlled potentiometer.

As illustrated, each channel is independently programmable with a 10 mA maximum amplitude (50 μA resolution). The timing resolution of the arbitrary waveform generator is 100 μs, which is mainly imposed by (a) the delay due to command communication through the wireless link, and (b) the delay for programming digital potentiometers. Out of the two, the communication delay is largely dominant compared to the approximately $<10\mu s$ delay of the digital potentiometers. Therefore, it should be considered that the $100\mu s$ limit is only valid if we want to program the stimulation current amplitude *on-the-fly* and *wirelessly*. Otherwise, a preprogrammed arbitrary waveform stimulation can be generated by the presented design with a minimum pulse-width of $10\mu s$. The pulse-width chosen for the waveforms shown in Fig. 6 are

typical widths that are requested by our clinician collaborators, for the targeted application (epilepsy animal model). For electrical stimulation, the typical stimulation frequency is 5-30 Hz. Considering the 0.25-0.3% duty cycle (frequency dependent) used for these pulses, their widths is in the range of 100-500 μs.

Fig. 7 shows the adaptive power supply value when the load impedance is changed in small steps from 100 Ω to 5 kΩ and then back to 100 Ω. As shown, the supply voltage increases with a maximum delay of 1ms/V, and is followed by the mid-range voltage V_{MID} used for the reference electrode. The adaptive supply loop requires a short period of time to calculate and generate a new value for the supply voltage. The calculation delay is negligible compared to the voltage generation delay. For voltage generation, the delay varies depending on how much difference is between the present supply voltage value and the targeted value. The limit for the rate of change (1ms/V) comes from the time constant of the charging/discharging of the on-board super capacitor and the excess current provided by the inductive power receiver.

Figure 8 depicts the comparison of system power consumption in two cases of with and without the adaptive supply control, for different electrode impedances. As shown, for a fixed stimulation current amplitude, adaptive supply voltage could result in saving up to 70% of the total power consumption, which would be wasted otherwise. Fig. 9(a) shows how the stimulation current driver output varies when the digitally-controlled potentiometer in series with a common-base BJT emitter varies from 20 kΩ to 60 Ω. Fig. 9(b) shows the anodic and cathodic current amplitudes generated by the stimulator for different resistor values. To evaluate the device performance considering both tissue safety and energy efficiency, a figure of merit (FoM) proposed in [54] is used. The FoM is defined as [54],

$$FoM = \frac{E_{ECS}}{N \times 2^{SENOB}} \quad (2)$$

where E_{ECS} is the stimulator energy efficiency, N is the number of independent channels, and SENOB is the stimulator effective number of bits, which represents its dynamic range in current generation. For this device, thanks to the adaptive supply system, the E_{ECS} is close to unity (0.83< E_{ECS} <0.92). For a typical stimulation frequency of 20Hz, I_{DC}=15μA, resulting in a $Q_{residual}$=750nC. Also considering the maximum current amplitude of 10mA, and for the same stimulation frequency, the Q_{cath}=250nC. The above yields a SENOB=8.4, and a FoM=2.5$\times10^{-3}$.

VII. IN VIVO EXPERIMENTAL RESULTS

Being capable of multi-channel stimulation with both electrical and optical agents, the neurostimulator implant could be used as an exploratory device in optogenetic experiments, as well as an alternative treatment option for various neurological diseases that require electrical stimulation, especially with high voltage compliance. Integrated with the in-house-fabricated flexible electrode that provides 16 channel electrical recording and 2 channel optical stimulation, it provides the means to perform optical stimulation on genetically-modified
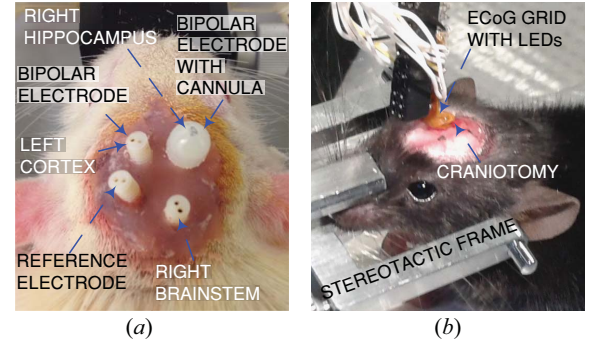

Fig. 10: (a) Microelectrode chronic implantation and (b) placement of LEDs assembled within a flexible Optical/ECoG electrode array (opcog) through a craniotomy on the cortex.
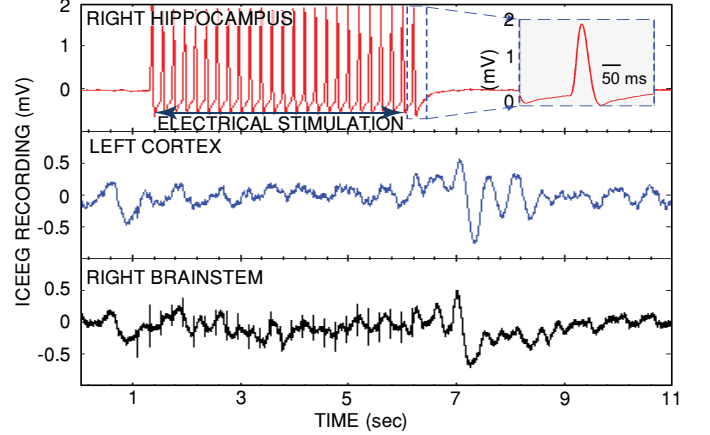

Fig. 11: Electrical stimulation of the hippocampus and icEEG recordings in the hippocampus, cortex and brainstem.
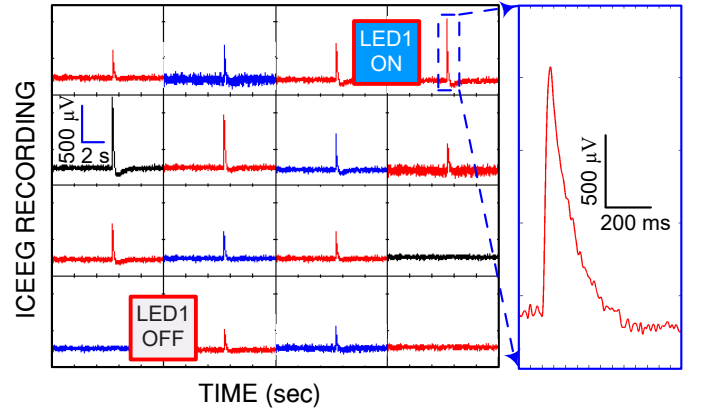

Fig. 12: A brief (30 ms) optical stimulation using LED1 and spatiotemporal propagation of neuronal excitation in a ChR2-expressing mouse.

brain cells and monitor the neural excitation (e.g. seizure generation in case of an epilepsy model) simultaneously. As for a treatment device, it could be paired with a neuro-monitoring/neurostimulation device (e.g., the device reported in [49]) and provide current-mode electrical stimulation with high voltage compliance for applications that require stimulating to a high-impedance load, or stimulating with high current amplitude such as muscle stimulation.

Two separate in-vivo experiments were performed to validate the stimulator's functionality for electrical and optical

stimulation. The procedures for both experiments were approved by the ethics committee of the Hospital for Sick Children and the Toronto Western Research Institute. The experiments were conducted at the Neuroscience and Mental Health Research Institute and Toronto Western Research Institute, for electrical and optical stimulation, respectively. For the electrical stimulation in-vivo experiment, the device was mounted on a rodent that could freely move. However, for the optical stimulation in-vivo experiment, since a smaller rodent model was used (mouse) the device was not light enough to be mounted on the animal and the experiment had to be done with the animal being held to a fixed position.

The choice of a mouse animal model for the optical stimulation experiment was mainly due to the availability of the proof-of-concept from [57] showing the efficacy of optical stimulation in inducing epileptic seizures in that specific transgenic animal model, which was used as the ground truth to evaluate the efficacy of the presented wearable medical device in inducing seizures. It should be noted that the device wireless connectivity (power and data) for conducting experiment with a freely-moving animal is validated through the electrical stimulation experiment. Therefore, since the power requirements as well as the Tx-Rx coil separation of the electrical stimulation experiment exceeds the optical one, we expect the same (or better) performance for the wireless connectivity (power and data) of the device when used for conducting optical stimulation on a freely-moving animal.

Two types of electrodes were used for the in-vivo experiments. The one shown in Fig. 10(a) is used for electrical stimulation to suppress epileptic seizures. The electrode shown in Fig. 5 and Fig. 10(b) which has 16 recording channels and 2 optical stimulation sources is used for the second in-vivo experiment which does optical stimulation for the purpose of seizure induction in genetically-modified brain cells.

For the electrical stimulation experiment (with rats) the device was mounted on the animal, and it was connected to the backend of the recording/stimulation electrodes using FFC (flexible flat cable) and 16-channel Molex connectors (Molex-5034801600). Same type of cables and connectors (only with 8 leads (Molex-5034800800)) were used for the optogenetic experiment to control the LEDs and to connect to the backend of the recording electrodes.

A. Electrical Stimulation

The electrical stimulator was validated by stimulating on a Wistar rat (250 gm) hippocampus in an in vivo chronic experiment. For this purpose, four bipolar microelectrodes were implanted into right the hippocampus, left cortex, right brainstem, and the skull as a reference. The hippocampus was stimulated and icEEG (intra-cranial electroencephalogram) from the hippocampus, cortex and brainstem were recorded (sampling rate: 1.7 kSps) using a commercial amplifier (Biopac Inc.). In the chronic experiment, the electrical stimulator triggered pulses with 150 μs width and 200 μA current at 5 Hz for 5 seconds into the hippocampus. The stimulation effect propagated to the brainstem quickly, which partially inhibited cortical activity (shown in Fig. 11).

B. Optical Stimulation and Electrical Recording

In the second experiment, the optical stimulator was tested by shining blue light on the cortex of a transgenic mouse (50 days old) in vivo. Procedures involving animals have been previously described [57] were performed in accordance with the guidelines of the Canadian Council on Animal Care and approved by the Institutional Animal Care Committee. In brief, a VGAT-ChR2 mouse was obtained from The Jackson Laboratory (JAX; Maine, USA) expressed channel rhodopsin in all GABAergic interneuronal subtypes [55], [56]. Ketamine (95 mg/kg) and Xylazine (5 mg/kg) were used to anesthetize the mouse before it was mounted into a stereotactic frame. Local anesthesia (Lidocaine) was applied into the periosteum and eye ointment was applied to the mouses eyes. The scalp was then removed to expose the skull. A 4-mm diameter craniotomy was then performed (at 2.0 mm latero-medial and -2.0 mm rostro-caudal) to expose the somatosensory cortex.

To induce recurrent electrographic seizures, 4-Aminopyridine (4-AP) was dissolved in saline (1.5 mM) and topically applied onto the exposed cortex for 10–15 mins [42], [56], [57]. The opcog (ECoG electrode with optical stimulation capability) was then placed on the somatosensory cortex through the 4–mm diameter craniotomy.

Initially, the stimulator triggered a blue light pulse for 30 ms and the icEEG was recorded using ECoG electrode array contacts. The blue light triggered neural spikes around the LED, and these spikes gradually propagated to distant regions within an approximately 1 mm distance. Figure 12 shows the recorded data from the 16 recording sites of the electrode array. The two LEDs are shown in the way they are physically located with respect to the recording sites. For the LEDs, the blue color means the LED is on, and white means it is off. This figure shows the result of the experiment where a brief (30 ms) optical stimulation is performed by one of the LEDs (LED1).

For the actual experiment, photostimulation (470 nm) of various durations (1–20 s) was delivered at a fixed interstimulus interval (period) of 300 s, a value close to the intrinsic rate at which electrographic seizures occurred spontaneously. For electrographic seizures, the onset was defined as the LVF onset pattern and the offset was defined to be when rhythmic, high-amplitude ictal activity ceased.

Figure 13(a) and 13(b) shows two examples of 4-channel recordings of the brain neural activity before, during and after 5 s and 20 s optogenetic stimulations, respectively. As shown, the low voltage fast ictal activity is observed immediately after conclusion of the optical stimulation pulse. Control experiments were repeated with C57BL/6 mice to test for any photoelectric effects or photostimulus-induced phenomenon (unrelated to ChR2 depolarization) in the naive brain tissue. Figure 13(c) shows an example of control experiment results where no ictal activity is observed following the optical stimulation.

VIII. Conclusion

A wireless hybrid current-mode and optical-mode miniature neurostimulating system is presented. The 16-channel electrical stimulator outputs arbitrary-waveform charge-balanced
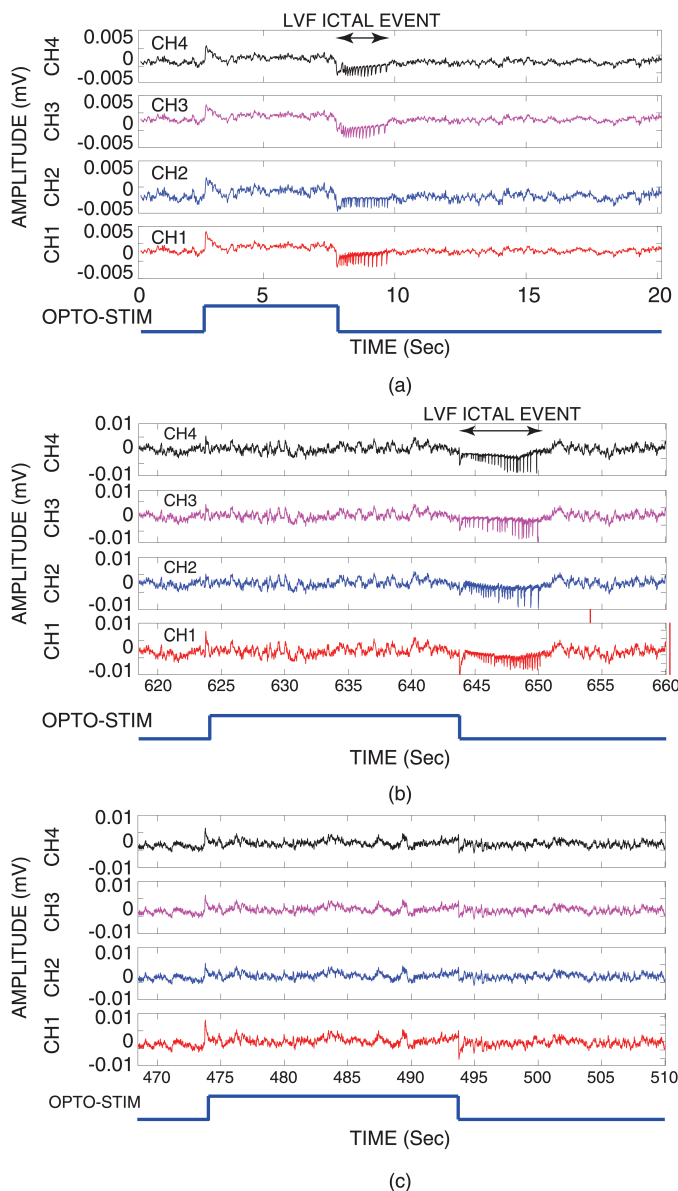
Fig. 13: Four channel recordings of brain neural activity before, during and after (a) 5s and (b) 20 s optical stimulation in an epileptic animal, illustrating post-stimulation LVF ictal brain activity. (c) Four channel recordings of brain neural activity before, during and after 20 s optical stimulation in a control animal, with no post-stimulation LVF activity, indicating the absence of photo-electric effect.

current-mode stimulation pulses with the amplitude ranging from 50 μA to 10 mA and voltage compliance up to 24 v. To save power, the system continuously monitors the varying electrode impedance and adjusts its supply voltage accordingly. The 8-channel optical stimulator reuses the arbitrary-waveform generation functions of the electrical stimulator, and drives 8 LEDs with a maximum of 25 mA. The dual-mode neurostimulator is connected to a wireless power/data communication board and a flexible 32-layer coil, to form a $3 \times 2.5 \times 1$ cm^3 wireless implantable device. To perform simultaneous optical stimulation and electrical recording, a custom-made

array of 4×4 ECoG electrodes and 8 LEDs (300 μm pitch) is fabricated, allowing for multi-channel optical stimulation and simultaneous monitoring of the neural response by the ECoG electrodes, at different distances of the stimulation site. Both electrical and optical stimulation results from chronic and acute in vivo rodent experiments are presented.

IX. ACKNOWLEDGMENT

REFERENCES

[1] G. Regesta, P. Tanganelli, " Clinical aspects and biological bases of drug-resistant epilepsies," Epilepsy research. 1999, 34(2): 109–22.

[2] R. S. Fisher and A. L. Velasco, "Electrical brain stimulation for epilepsy," Nat Rev Neurol, vol. 10, pp. 261–70, May 2014.

[3] F. T. Sun and M. J. Morrell, "The RNS System: responsive cortical stimulation for the treatment of refractory partial epilepsy," Expert Rev Med Devices, vol. 11, pp. 563–72, Nov 2014.

[4] H. Khosravani, P. L. Carlen, J. L. Perez Velazquez, "The control of seizure-like activity in the rat hippocampal slice," Biophys J, vol. 84, pp. 687–95, Jan 2003.

[5] P. Rajdev, M. Ward, P. Irazoqui, "Effect of stimulus parameters in the treatment of seizures by electrical stimulation in the kainate animal model," Int J Neural Syst, vol. 21, pp. 151–62, Apr 2011.

[6] C. Hamani, M. Hodaie, J. Chiang, M. Del Campo, D. M. Andrade, D. Sherman, M. Mirski, L. E. Mello, A. M. Lozano, "Deep brain stimulation of the anterior nucleus of the thalamus: effects of electrical stimulation on pilocarpine-induced seizures and status epilepticus," Epilepsy Res, vol. 78, pp.117–23, 2008.

[7] H. Kassiri, A. Bagheri, N. Soltani, K. Abdelhalim, H. Jafari, M. T. Salam, J. L. P. Velazquez and R. Genov, H. " Battery-less tri-band-radio neuro-monitor and responsive neurostimulator for diagnostics and treatment of neurological disorders," IEEE J. Solid-State Circuits, vol. 51, no. 5, pp. 1274-1289, May 2016.

[8] H. Kassiri, M. T. Salam, M. R. Pazhouhandeh, N. Soltani, J. L. Perez Velazquez, P. L. Carlen, R. Genov, "Rail-to-Rail-Input Dual-Radio 64-channel Closed-Loop Neurostimulator," IEEE Journal of Solid-State Circuits, Vol. 52, No. 11, pp. 2793-2810, Oct. 2017.

[9] Rodriguez-Oroz, M. C., J. A. Obeso, A. E. Lang, J-L. Houeto, P. Pollak, Stig Rehncrona, J. Kulisevsky et al. "Bilateral deep brain stimulation in Parkinson's disease: a multicentre study with 4 years follow-up," Brain, Vol. 128, no. 10, 2005, pp. 2240–2249.

[10] H. Kassiri, S. Tonekaboni, M. T. Salam, N. Soltani, K. Abdelhalim, J. L. Perez Velazquez, R. Genov, "Closed-Loop Neurostimulators: A Survey and a Seizure-Predicting Design Example for Intractable Epilepsy Treatment," IEEE Transactions on Biomedical Circuits and Systems, Vol. 11, No. 5, pp. 1026-1040, Oct. 2017.

[11] Y. Schiller, and Y. Bankirer, "Cellular mechanisms underlying antiepileptic effects of low-and high-frequency electrical stimulation in acute epilepsy in neocortical brain slices in vitro," Journal of neurophysiology, Vol. 97, no. 3, 2007, pp. 1887–1902.

[12] M. T. Salam, J. L. Perez Velazquez, R. Genov, "Comparative Analysis of Seizure Control Efficacy of 5Hz and 20Hz Responsive Deep Brain Stimulation in Rodent Models of Epilepsy,", IEEE BioCAS 2015

[13] M. T. Salam, H. Kassiri, R. Genov, J. L. Perez Velazquez, "Rapid brief feedback intracerebral stimulation based on realtime desynchronization detection preceding seizures stops the generation of convulsive paroxysms," Epilepsia 56 (8), 1227–1238

[14] A. R. Adamantidis, F. Zhang, A. M. Aravanis, K. Deisseroth, L. De Lecea, "Neural substrates of awakening probed with optogenetic control of hypocretin neurons," Nature Vol. 450, No. 7168 pp. 420–424, 2007.

[15] A. Witt, A. Palmigiano, A. Neef, A. El Hady, F. Wolf, D. Battaglia "Controlling the oscillation phase through precisely timed closed-loop optogenetic stimulation: a computational study," Frontiers in neural circuits, Vol. 7, 2013.

[16] G. Gagnon-Turcotte, M. Noormohammadi Khiarak, Ch. Ethier, Y. De Koninck, and B. Gosselin. "A 0.13-μm CMOS SoC for Simultaneous Multichannel Optogenetics and Neural Recording." IEEE Journal of Solid-State Circuits, Vol. 99, pp. 1-14, 2018.

[17] R. Ramezani, Y. Liu, F. Dehkhoda, A. Soltan, D. Haci, H. Zhao, D. Firfilionis et al, "On-Probe Neural Interface ASIC for Combined Electrical Recording and Optogenetic Stimulation," IEEE Transactions on Biomedical Circuits and Systems, vol.12, Issue 3, 2018.

[18] Y. Jia, S. A. Mirbozorgi, B. Lee, W. Khan, F. Madi, A. Weber, W. Li, and M. Ghovanloo. "A mm-sized free-floating wirelessly powered implantable optical stimulating system-on-a-chip." In Solid-State Circuits Conference (ISSCC), 2018 IEEE International, pp. 468-470. IEEE, 2018.

[19] E. Noorsal, K. Sooksood, H. Xu, R. Hornig, J. Becker, and M. Ortmanns, "A neural stimulator frontend with high-voltage compliance and programmable pulse shape for epiretinal implants," Solid-State Circuits, IEEE Journal of 47, no. 1 (2012): 244–256.

[20] H. Kassiri, G. Dutta, N. Soltani, Ch. Liu, Y. Hu, and R. Genov "An impedance-tracking battery-less arbitrary waveform neurostimulator with load-adaptive 20V voltage compliance," in Proc. IEEE ESSCIRC, Sep. 2016, pp. 225-228.

[21] H. M. Lee, K. Y. Kwon, W. Li, M. Ghovanloo, "A Power-Efficient Switched-Capacitor Stimulating System for Electrical/Optical Deep Brain Stimulation," Solid-State Circuits, IEEE Journal of 50.1 (2015): 360–374.

[22] H. Kassiri, M. R. Pazhouhandeh, J. L. P. Velazquez, R. Genov, "All-Wireless 64-channel 0.013mm2/ch Closed-Loop Neurostimulator with Rail-to-Rail DC Offset Removal," IEEE International Solid-State Circuits Conference (ISSCC'2017), Feb. 2017.

[23] H. Kassiri, A. Bagheri, N. Soltani, K. Abdelhalim, H. M. Jafari, M. T. Salam, J. L. Perez Velazquez, R. Genov, "Inductively-Powered Direct-Coupled 64-Channel Chopper-Stabilized Epilepsy-Responsive Neurostimulator with Digital Offset Cancellation and Tri-Band Radio," IEEE ESSCIRC, 2014, pp. 95–98.

[24] H. Kassiri, M. T. Salam, F. D. Chen, B. Vatankhah, N. Soltani, M. Chang, P. Carlen, T. A. Valiante, R. Genov, "Implantable Arbitrary-Waveform Electro-Optical Stimulator with an Inductively-Powered Load-Adaptive High-Voltage Supply," IEEE Biomedical Circuits and Systems Conference (BioCAS 2015), Atlanta, Oct. 2015.

[25] DW. Grasse, S. Karunakaran, K. A. Moxon, "Neuronal synchrony and the transition to spontaneous seizures," Experimental neurology. 2013 Oct, 248:72–84.

[26] V. Gnatkovsky, L. Librizzi, F. Trombin, M. de Curtis, "Fast activity at seizure onset is mediated by inhibitory circuits in the entorhinal cortex in vitro," Ann Neurol. 2008 Dec, 64(6):674–86.

[27] B. Lasztoczi, G. Nyitrai, L. Heja, J. Kardos, "Synchronization of GABAergic inputs to CA3 pyramidal cells precedes seizure-like event onset in juvenile rat hippocampal slices," Journal of neurophysiology. 2009 Oct, 102(4):2538–53.

[28] J. L. Velazquez, P. L. Carlen, "Synchronization of GABAergic interneuronal networks during seizure-like activity in the rat horizontal hippocampal slice," The European journal of neuroscience. 1999 Nov, 11(11):4110–8.

[29] L. Uva, G. L. Breschi, V. Gnatkovsky, S. Taverna, M. de Curtis, "Synchronous inhibitory potentials precede seizure-like events in acute models of focal limbic seizures," The Journal of neuroscience : the official journal of the Society for Neuroscience, 2015 Feb 18, 35(7):3048–55.

[30] M. Dantuono, M. J. Louvel, R. Khling, D. Mattia, A. Bernasconi, A. Olivier, B. Turak, A. Devaux, R. Pumain, M. Avoli, "GABAA receptordependent synchronization leads to ictogenesis in the human dysplastic cortex," Brain. 2004, 127(7):1626–40.

[31] D. Mattia, A. Olivier, M. Avoli, "Seizurelike discharges recorded in human dysplastic neocortex maintained in vitro," Neurology, 1995, 45(7):1391–5.

[32] M. Avoli, M. de Curtis, "GABAergic synchronization in the limbic system and its role in the generation of epileptiform activity," Progress in neurobiology, 2011, 95(2):104–32.

[33] M. De Curtis, V. Gnatkovsky, "Reevaluating the mechanisms of focal ictogenesis: The role of lowvoltage fast activity," Epilepsia, 2009, 50(12):2514–25.

[34] Z. Shiri, F. Manseau, M. Levesque, S. Williams, M. Avoli, "Interneuron activity leads to initiation of low-voltage fast-onset seizures," Ann Neurol. 2015 Mar, 77(3):541–6.

[35] A. L. Velasco, C. L. Wilson, T. L. Babb, J. Engel, "Functional and anatomic correlates of two frequently observed temporal lobe seizure-onset patterns," Neural plasticity, 2000, 7(1-2):49–63.

[36] L. Wittner, L. Eross, S. Czirjak, P. Halasz, T. F. Freund, Z. Magloczky, "Surviving CA1 pyramidal cells receive intact perisomatic inhibitory input in the human epileptic hippocampus," Brain, 2005 Jan, 128(Pt 1):138–52.

[37] R. Cossart, C. Dinocourt, J. C. Hirsch, A. Merchan-Perez, J. De Felipe, Y. Ben-Ari, M. Esclapez, c. Bernard, "Dendritic but not somatic GABAergic inhibition is decreased in experimental epilepsy, Nature neuroscience," 2001 Jan, 4(1):52–62.

[38] A. Klaassen, J. Glykys, J. Maguire, C. Labarca, I. Mody, J. Boulter, "Seizures and enhanced cortical GABAergic inhibition in two mouse models of human autosomal dominant nocturnal frontal lobe epilepsy," Proceedings of the National Academy of Sciences of the United States of America, 2006 Dec 12, 103(50):19152–7.

[39] I. Marchionni, G. Maccaferri, "Quantitative dynamics and spatial profile of perisomatic GABAergic input during epileptiform synchronization in the CA1 hippocampus," The Journal of physiology, 2009 Dec 1, 587(Pt 23):5691–708.

[40] D. A. Prince, K. Jacobs, "Inhibitory function in two models of chronic epileptogenesis," Epilepsy research, 1998 Sep, 32(1–2):83–92.

[41] L. Yekhlef, G. L. Breschi, L. Lagostena, G. Russo, S. Taverna, "Selective activation of parvalbumin- or somatostatin-expressing interneurons triggers epileptic seizurelike activity in mouse medial entorhinal cortex," Journal of neurophysiology, 2015 Mar 1, 113(5):1616–30.

[42] L. M. Ritter, P. Golshani, K. Takahashi, S. Dufour, T. Valiante, M. Kokaia, "WONOEP appraisal: optogenetic tools to suppress seizures and explore the mechanisms of epileptogenesis," Epilepsia. 2014 Nov, 55(11):1693–702.

[43] Y. Ben-Ari, E. Cherubini, R. Corradetti, J. L. Gaiarsa, "Giant synaptic potentials in immature rat CA3 hippocampal neurones," The Journal of physiology, 1989 Sep, 416:303–25.

[44] P. Bregestovski, C. Bernard, "Excitatory GABA: how a correct observation may turn out to be an experimental artifact," Frontiers in pharmacology. 2012, 3.

[45] F. Shahrokhi, K. Abdelhalim, D. Serletis, P. L. Carlen, R. Genov, "The 128-channel fully differential digital integrated neural recording and stimulation interface," IEEE Trans. Biomed. Circuits Syst., vol. 4, no. 3, pp. 149–161, Jun. 2010.

[46] S. K. Arfin, and R. Sarpeshkar, "An energy-efficient, adiabatic electrode stimulator with inductive energy recycling and feedback current regulation," Biomedical Circuits and Systems, IEEE Transactions on 6, no. 1 (2012): 1–14.

[47] I. Williams, and T. G. Constandinou, "An energy-efficient, dynamic voltage scaling neural stimulator for a proprioceptive prosthesis," Biomedical Circuits and Systems, IEEE Transactions on 7, no. 2 (2013): 129–139.

[48] Sh. Kelly, and J. L. Wyatt, "A power-efficient neural tissue stimulator with energy recovery," Biomedical Circuits and Systems, IEEE Transactions on 5, no. 1 (2011): pp. 20–29.

[49] H. Kassiri, N. Soltani, M. T. Salam, R. Genov, J. P. Velazquez, "Battery-less Modular Responsive Neurostimulator for Prediction and Abortion of Epileptic Seizures," IEEE International Symposium on Circuits and Systems (ISCAS) 2016.

[50] M. T. Salam, H. Kassiri, N. Soltani, R. Genov, "Tradeoffs Between Wireless Communication and Computation in Closed-loop Implantable Devices," IEEE International Symposium on Circuits and Systems (ISCAS) 2016.

[51] A. Wongsarnpigoon, J. P. Woock, W. M. Grill, "Efficiency analysis of waveform shape for electrical excitation of nerve fibers," IEEE Transaction on Neural Systems and Rehabilitation Engineering, vol. 18, no. 3, pp. 319–328, June 2010.

[52] A. Wongsarnpigoon and W. M. Grill, "Energy-efficient waveform shapes for neural stimulation revealed with a genetic algorithm," J. Neural Eng., vol. 7, no. 4, June 2010

[53] N. Soltani, M. S. Aliroteh, R. Genov, "Cellular Inductive Powering System for Weakly-Linked Resonant Rodent Implants," IEEE BioCAS, 2013.

[54] F. Kolbl, and A. Demosthenous, " A figure of merit for neural electrical stimulation circuits," Engineering in Medicine and Biology Society (EMBC), 37th Annual International Conference of the IEEE, pp. 2075–2078. IEEE, 2015.

[55] S. Zhao, J. T. Ting, H. E. Atallah, L. Qiu, J. Tan, B. Gloss, G. J. Augustine et al., "Cell type-specific channelrhodopsin-2 transgenic mice for optogenetic dissection of neural circuitry function," Nature methods, 2011, Vol. 8, No. 9, pp.745–752.

[56] N. Rensing, Y. Ouyang, X. F. Yang, K. A. Yamada, S. M. Rothman, M. Wong, "In vivo imaging of dendritic spines during electrographic seizures," Annals of neurology, 2005, Vol. 58, No. 6, pp.888–898.

[57] M. Chang, J. A. Dian, S. Dufour, L. Wang, H. Moradi Chameh, M. Ramani, L. Zhang, P. L. Carlen, T. Womelsdorf, and Taufik A. Valiante. "Brief activation of GABAergic interneurons initiates the transition to ictal events through post-inhibitory rebound excitation," Neurobiology of disease, Vol. 109,2018, pp.102–116.